

# A Low-Cost High-Gain Dual-Beam Antenna With Large Beam Tilt Angle for Through-Wall FTTR Applications

Dian Li, Xulin Xu, Long Zhang, *Member, IEEE*, Hao Xiong, Dongwei Wu, Francis Keshmiri, Xiang Wang, Wenchao Liu, Yejun He, *Senior Member, IEEE*, Steven Gao, *Fellow, IEEE*

**Abstract**—In this letter, a high-gain dual-beam antenna with large beam tilt angle is proposed as a cost-effective solution for through-wall fiber-to-the-room (FTTR) applications. The dual-beam radiation is realized by the anti-phase currents distribution on the antenna, and two pairs of parasitic elements are loaded to significantly elevate the beam tilt angle and improve the bandwidth. The measured bandwidth of the proposed antenna is 1100 MHz (4.88-5.98 GHz), well covering the FTTR operation bands. Besides, the maximum tilt angle for the symmetrical dual beams reaches  $53^\circ$ , and the peak gain is 10.05 dBi at 5.3 GHz. Moreover, received signal strength indicator (RSSI) and throughput experiments are conducted to verify the efficacy of the proposed antenna in terms of through-wall functionality. The experimental results demonstrate that the proposed antenna exhibits superior through-wall and multi-room coverage capability in comparison to the conventional monopole antenna.

**Index Terms**—Dual-beam antenna, FTTR antenna, high gain, large beam tilt angle, multi-room coverage, through-wall.

## I. INTRODUCTION

IN scenarios where rooms are arranged closely, such as dormitories and hotels, the propagation of electromagnetic waves will be greatly attenuated across the walls of adjacent rooms, leading to a wireless access point (AP) equipped per room for better communication service. Therefore, the deployment of a single AP to cover multiple rooms has received considerable interests due to the significant reduction of network construction cost [1]. Dual-beam antennas are well-suited for wireless systems that require the coverage of multiple areas simultaneously [2]. As illustrated in Fig. 1, a ceiling-mounted dual-beam antenna with large beam tilt angle and high antenna gain can effectively extend the signal coverage area from one room to three rooms. However, achieving signal coverage over such an extensive area is quite challenging for antenna design: 1) The dual beams of the antenna need to have a large beam tilt angle (approximately  $50^\circ$  to  $55^\circ$ ) to cover rooms on both sides of a wall; 2) It is imperative that the

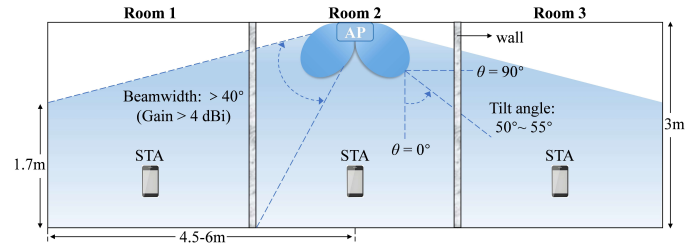


Fig. 1. Schematic of multi-room coverage utilizing high-gain dual-beam antennas. (Adjacent rooms are separated by a wall)

antenna possesses high gain over a wide beamwidth for better through-wall coverage [3], [4], specifically the beamwidth with gain  $> 4$  dBi should be greater than  $40^\circ$ ; 3) The bandwidth of the antenna needs to cover the fiber-to-the-room (FTTR) 5 GHz band while the antenna structure needs to be as simple as possible for cost and compatibility purpose.

Usually, dual-beam radiation can be achieved by elaborately designed back-to-back end-fire antennas [5]–[8], phased array antennas [9]–[13], leaky-wave antennas [14]–[18], and microstrip antennas [19]–[24]. For back-to-back end-fire antennas, the dual beams pointing to opposite directions are incapable of covering multiple rooms when the antenna is installed on the rooftop. Phased array antennas are not suitable for ceiling-mounted applications due to their complex and costly system architecture, while leaky-wave antennas are incompatible for FTTR scenarios where the spectrum resources are quite limited for each channel. Although microstrip antennas have been widely used to generate dual-beam radiation, they suffer from drawbacks of narrow bandwidth, small beam tilt angle and low antenna gain. A dual-beam antenna with large beam tilt angle was reported in [25]. However, the antenna is comprised of six independent steel plates and a feeding network on the ground plane, which renders it disadvantageous in terms of design simplicity, fabrication cost, and assembly accuracy, and not applicable to practical applications.

Based on the above discussion, this letter proposes a high-gain, broadband, dual-beam antenna with large beam tilt angle for through-wall FTTR applications. The dual-beam radiation is realized by exciting two anti-phase currents, then two pairs of parasitic elements are introduced to further elevate the beam tilt angle and extend the bandwidth. The measured results show that the antenna can achieve symmetrical dual beams with a beam tilt angle greater than  $50^\circ$  and the realized gain exceeding 9 dBi within the 5-5.9 GHz band. Comprehensive system experiments including the received signal strength indicator (RSSI) and throughput measurements verify the antenna as an excellent solution for through-wall FTTR applications.

This work was supported in part by the Shenzhen Science and Technology Program under grant JCYJ20230808105510020, and in part by Huawei under grant No. TC20230808040. (Corresponding author: Long Zhang.)

Dian Li, Xulin Xu, Long Zhang, and Yejun He are with the College of Electronics and Information Engineering, Shenzhen University, Shenzhen 518060, China (e-mail: long.zhang@szu.edu.cn).

Hao Xiong, Dongwei Wu, Francis Keshmiri, Xiang Wang are with Huawei Technologies Co., Ltd. Shenzhen, China (e-mail: xionghao30@huawei.com, wudongwei2@huawei.com, francis.keshmiri@huawei.com, eric.wangxiang@huawei.com).

Wenchao Liu is with the Home Network Department, E-surfing Digital Life Technology, China Telecom, Shanghai, China (e-mail: liuwc\_dys.sh@chinatelecom.cn).

S. Gao is with the Department of Electronic Engineering, The Chinese University of Hong Kong, Hong Kong (e-mail: scgao@ee.cuhk.edu.hk).

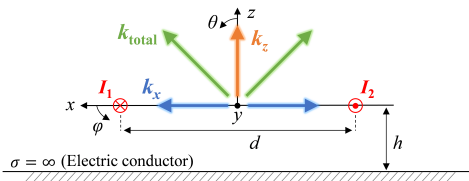


Fig. 2. Illustration of two anti-phase electric currents array.

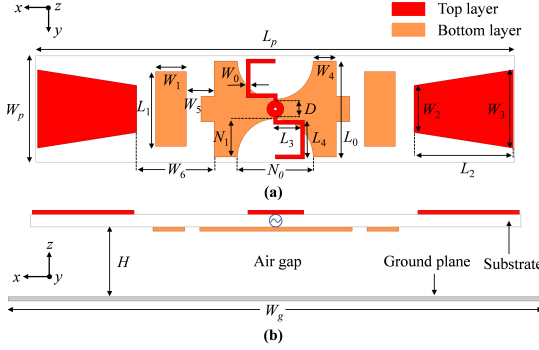


Fig. 3. Configuration of the dual-beam antenna. (a) Top view. (b) Side view. Design parameters (unit: mm):  $L_p = 96$ ,  $W_p = 21$ ,  $W_0 = 0.8$ ,  $W_1 = 6.2$ ,  $W_2 = 9.5$ ,  $W_3 = 15.8$ ,  $W_4 = 4.6$ ,  $W_5 = 5.6$ ,  $W_6 = 15.5$ ,  $W_g = 126$ ,  $L_0 = 19.3$ ,  $L_1 = 15$ ,  $L_2 = 20$ ,  $L_3 = 5.5$ ,  $L_4 = 7$ ,  $N_0 = 15.2$ ,  $N_1 = 7.6$ ,  $D = 3.4$ ,  $H = 14.5$ .

## II. ANTENNA DESIGN AND PRINCIPLE

Let us consider a two-element array made up of two anti-phase electric currents placed along the  $y$ -axis direction, as shown in Fig. 2. The far-field pattern of a single electric current is defined as [26]

$$E_0(\varphi) = j\eta \frac{kI_0 l \cos \varphi}{4\pi r} e^{-jkr} \quad (1)$$

where  $\eta$  is the wave impedance,  $k = 2\pi/\lambda$  is the free-space wavenumber,  $I_0$  is the current amplitude,  $l$  is the current length. Then, the array factor for the two elements array with the same magnitude and phase difference  $\beta$  is

$$AF = \cos \left[ \frac{1}{2} (kd \sin \theta \cos \varphi + \beta) \right] \quad (2)$$

where  $\beta = \pi$ . For the  $xz$ - and  $yz$ -plane,  $\varphi$  equals 0 and  $\pi/2$ , respectively. Thus, the total far-field patterns for the anti-phase currents in the two main planes are

$$E(\theta, \varphi)_{xz} = -E_0 \sin \left( \frac{kd}{2} \sin \theta \right), E(\theta, \varphi)_{yz} = 0 \quad (3)$$

If  $d \approx \lambda/2$ , then the maximum radiation is obtained in the  $x$ -axis direction (denoted by  $k_x$ ), while the radiation in the  $y$ -axis direction is canceled out. Once an electric conductor is placed underneath, the reflected waves induced by the conductor will be oriented along the  $z$ -axis direction (denoted by  $k_z$ ) according to the image theory. Thus, the total wave vector  $k_{total}$  is superposed by  $k_x$  and  $k_z$ , generating a tilted dual-beam radiation. By adjusting the radiation intensity along vector  $k_x$  and  $k_z$ , the beam tilt angle can be altered.

Based on the aforementioned principles and inspired by the horizontally polarized antenna presented in [27], a dual-beam antenna with improved bandwidth and gain is proposed. The

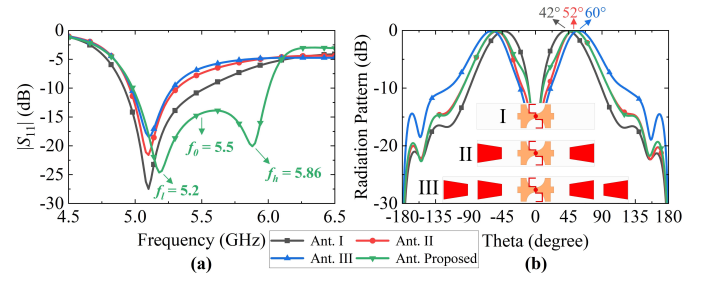


Fig. 4. (a) Simulated  $|S_{11}|$  of Ant. I, II, III and Proposed. (b) Simulated radiation patterns in  $xz$ -plane for Ant. I, II, III and Proposed at 5.1 GHz.

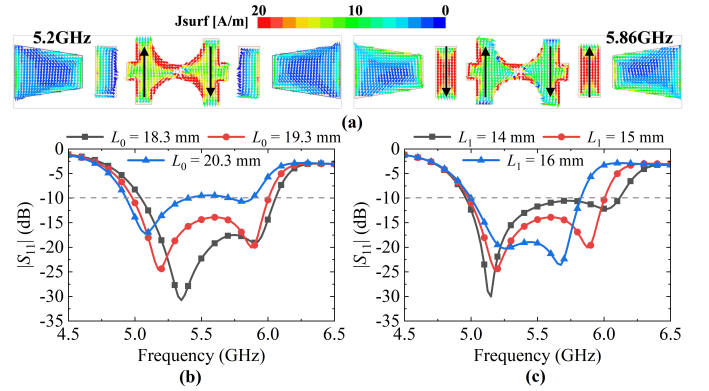


Fig. 5. (a) Current distributions of the proposed antenna at 5.2 and 5.86 GHz. (b) Simulated  $|S_{11}|$  for different  $L_0$ . (c) Simulated  $|S_{11}|$  for different  $L_1$ .

configuration of the proposed dual-beam antenna is shown in Fig. 3, which consists of a meander line, a notch radiator, two symmetrical rectangular strips, two symmetrical trapezoidal directors, and a ground plane. All elements are printed on a FR4 substrate ( $\epsilon_r = 4.4$ ) with a thickness of 0.762 mm. The ground plane is printed on another FR4 substrate, while two dielectric substrates are separated by an air gap with a height  $H$ , and a coaxial cable is used to feed the antenna directly.

The meander line provides differential excitation to the notch radiator, creating anti-phase electric currents on the radiator. Therefore, radiation nulls along the  $y$ -axis occur, while high-gain dual-beam radiation is generated in the  $x$ -axis direction. To illustrate the role of the trapezoidal directors, the antenna with only the notch radiator and the meander line is denoted as Ant. I. Ant. II refers to Ant. I plus a pair of trapezoidal directors, while Ant. III refers to Ant. I plus two pairs of trapezoidal directors. The trapezoidal shape is chosen over the rectangular one because its gradual taper can expand the operating bandwidth of the directors. As shown in Fig. 4, both Ant. I, Ant. II, and Ant. III resonate at 5.1 GHz, and the tilt angle of the symmetrical dual beams in the  $xz$ -plane is  $42^\circ$  for Ant. I,  $52^\circ$  for Ant. II and  $60^\circ$  for Ant. III. This indicates the trapezoidal directors can enhance the radiation intensity along vector  $k_x$ , thus elevating the beam tilt angle effectively. Similarly, the magnitude of  $k_z$  can be adjusted by changing the antenna height  $H$  to fine-tune the beam tilt angle. Meanwhile, loading the trapezoidal directors enhances the end-fire radiation, thereby improving the gain by about 1 dB. Since Ant. II has a suitable beam tilt angle that satisfies the system requirements, a single pair of trapezoidal directors is chosen.

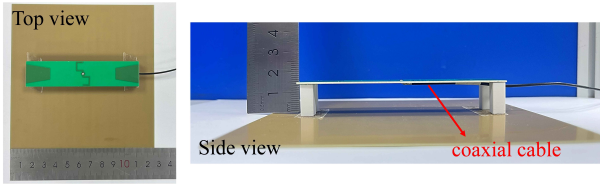


Fig. 6. Photographs of the fabricated dual-beam antenna.

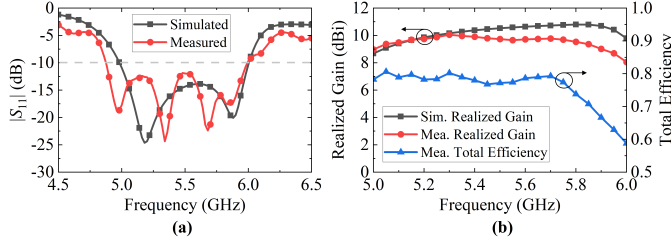


Fig. 7. Simulated and measured results of the proposed dual-beam antenna. (a)  $|S_{11}|$ . (b) Realized gain and total efficiency.

As the bandwidth of Ant. II is too narrow to cover the FTTR 5 GHz band (5.15–5.85 GHz), a pair of rectangular strips is added on either side of the notch radiator, which can introduce an additional resonance at 5.86 GHz ( $f_h$ ) while the resonance generated by the notch radiator only shifts slightly from 5.1 GHz to 5.2 GHz ( $f_l$ ). As shown in Fig. 5(a), the surface currents at 5.2 GHz are predominantly concentrated on the notch radiator, indicating that the radiation mainly comes from the notch radiator. Whereas at 5.86 GHz, the surface currents on the rectangular strips are significantly enhanced, indicating both the rectangular strips and the notch radiator contribute to the radiation, thus significantly expanding the bandwidth from 340 MHz (4.96–5.3 GHz) to 1000 MHz (5–6 GHz). It is necessary to note that the rectangular strips have a limited effect on the radiation pattern and the antenna gain.

The proposed antenna is, in principle, similar to the Yagi antenna. Thus, the initial dimensions of the antenna can be set as follows:  $L_0 \approx \lambda_l/2$ ,  $L_1 \approx \lambda_h/2$ ,  $N_0 + W_4 \times 2 \approx \lambda_0/2$ ,  $W_6 \approx \lambda_0/4$ ,  $W_2 < 0.4\lambda_h$ ,  $W_3 > 0.4\lambda_l$ ,  $L_2 \approx 0.4\lambda_0$  ( $\lambda_l$  and  $\lambda_h$  are the guided wavelength at  $f_l$  and  $f_h$ , respectively, while  $\lambda_0$  is the free-space wavelength at  $f_0$ ). Fig. 5 shows a further study on the length of the notch radiator ( $L_0$ ) and the rectangular strips ( $L_1$ ). As  $L_0$  increases, the resonance of the notch radiator is shifted to lower frequency, while the resonance of the rectangular strips is almost kept unchanged. Similarly, the resonance of the rectangular strips is moved to lower frequency when increasing  $L_1$ , while the resonance of the notch radiator remains essentially stable.

### III. ANTENNA MEASUREMENT RESULTS AND DISCUSSION

An antenna prototype is fabricated and measured as shown in Fig. 6. Fig. 7(a) shows the simulated and measured reflection coefficients, demonstrating bandwidths of 1000 MHz (5–6 GHz) and 1100 MHz (4.88–5.98 GHz), respectively. The difference between the simulated and measured reflection coefficients is caused by the fabrication and measurement errors, especially the possible reflections of the coaxial cable (25 cm long) and IPEX-to-SMA transition. As depicted in Fig.

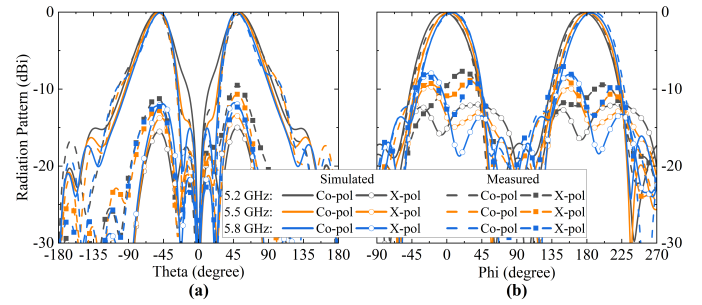


Fig. 8. Simulated and measured normalized radiation patterns of the proposed antenna in (a)  $xz$ -plane and (b)  $\theta = 52^\circ$  plane at 5.2, 5.5, and 5.8 GHz.

TABLE I  
COMPARISON WITH PREVIOUSLY REPORTED DUAL-BEAM ANTENNAS

Ref.	BW (%)	BTA ( $^\circ$ )	Gain (dBi)	Beamwidth ( $^\circ$ ) Ele./Azi.	Dimensions ( $\lambda_0^3$ )
[20]	13.2	32.5	8.87	$\sim 45$ /N.A.	$1.83 \times 1.28 \times 0.1$
[21]	12.7	31	7.7	$\sim 45$ /N.A.	$1.14 \times 0.7 \times 0.17$
[22]	23.5	30	6.8	$\sim 38$ /N.A.	$1.13 \times 0.42 \times 0.09$
[23]	7.3	33	9.6	$\sim 40$ /N.A.	$1.63 \times 1.63 \times 0.05$
[24]	6	46	7.3	$\sim 35$ /N.A.	$2.27 \times 2.27 \times 0.05$
[25]*	16	54	8.9	48/64	$1.76 \times 1.11 \times 0.24$
Prop. SG*	18.2	53	9.8	57/72	$1.76 \times 1.11 \times 0.24$
<b>Prop.</b>	<b>20.3</b>	<b>53</b>	<b>10.05</b>	<b>49/72</b>	<b><math>2.3 \times 2.3 \times 0.27</math></b>

\*: simulation results; BW: bandwidth; BTA: beam tilt angle; SG: small ground;  $\sim$ : approximately equal to; N.A.: not available; Ele.: elevation plane; Azi.: azimuth plane; Beamwidth refers to the beamwidth with gain  $> 4$  dBi.

7(b), the realized gain exceeds 9 dBi within the 5–5.9 GHz band, with a maximum gain of 10.05 dBi at 5.3 GHz. The total efficiency surpasses 70% within the 5–5.85 GHz band, with a maximum efficiency of 80.62% at 5.05 GHz.

The simulated and measured normalized radiation patterns at 5.2, 5.5, and 5.8 GHz in the  $xz$ -plane (elevation plane) and  $\theta = 52^\circ$  plane (azimuth plane) are shown in Fig. 8. The measured results demonstrate that the tilt angles of the symmetrical dual beams are all greater than  $50^\circ$  at various frequencies, with a maximum tilt angle of  $53^\circ$  at 5.2 GHz.

In addition to the beam tilt angle, beamwidth is also a critical metric for practical application. The measured beamwidths for gain  $> 4$  dBi in the  $xz$ -plane at 5.2, 5.5, and 5.8 GHz are  $49^\circ$ ,  $45^\circ$ , and  $43^\circ$ , respectively, satisfying the requirements delineated in Fig. 1. For the  $\theta = 52^\circ$  plane, the measured beamwidths are all greater than  $72^\circ$ . A comparison of the proposed and previously reported dual-beam antennas is tabulated in Table I. As revealed by Table I, the proposed antenna is superior to previous designs in terms of beam tilt angle, gain, and beamwidth. Although the proposed antenna has a large ground plane due to the system requirement, the antenna performance remains essentially unchanged except for a slight decrease in antenna gain under the same size as in [25].

### IV. RSSI AND THROUGHPUT EXPERIMENTAL RESULTS

A conventional monopole antenna with conical-beam radiation is fabricated and selected as the reference antenna for system experimental results comparison. The impedance bandwidth and the radiation patterns of the monopole antenna are shown in Fig. 9. Within the operation band of 5–6 GHz,



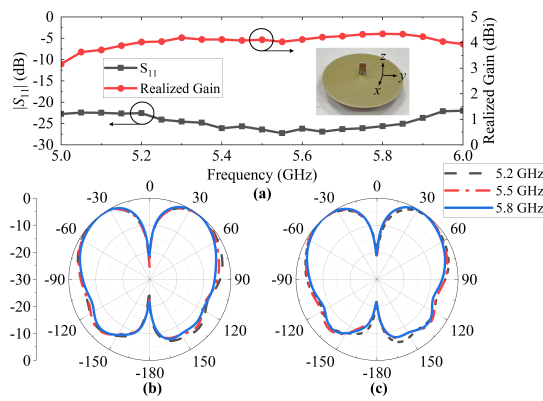


Fig. 9. Measured results of the monopole antenna. (a)  $|S_{11}|$  and realized gain. (b) and (c) normalized radiation patterns in  $xz$ - and  $yz$ -plane.

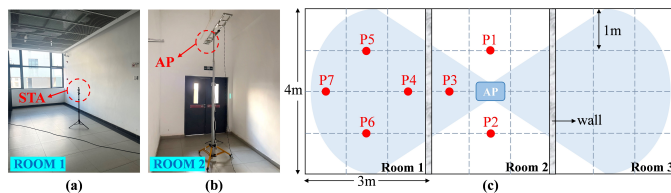


Fig. 10. Experimental scenarios for RSSI and throughput. (a) Room 1. (b) Room 2. (c) Top view of the testing scenario.

the measured  $|S_{11}|$  is less than -20 dB. Conical beams with a maximum gain around  $\theta = 40^\circ$  in both main planes are observed. The measured realized gain of the monopole antenna is greater than 4 dBi from 5.2 to 5.95 GHz.

The scenario shown in Fig. 10 is chosen for RSSI and throughput experiments. To better characterize the experimental results, each room is divided into 12 square cells. Due to the symmetry of the experimental site, only the left half is selected for results demonstration (Room 1 and Room 2). The AP, located at the center of Room 2, is placed 3 m above the ground and 1.5 m from the 25 cm-thick reinforced concrete wall. A mobile phone placed 1.2 m above the ground functions as a station (STA) to connect to the AP. The mean RSSI value over a one-minute period is measured at the center of each cell in Room 1 and Room 2, while throughput is measured at seven sampling points, as indicated by red dots in Fig. 10(c).

The distribution of RSSI in Room 1 and Room 2 is illustrated in Fig. 11. The omnidirectional radiation of the monopole antenna with a small beam tilt angle ensures effective signal coverage in a single room, therefore the RSSI levels of the dual-beam antenna within Room 2 is slightly lower than that of the monopole antenna due to the large beam tilt angle. Whereas in Room 1, the RSSI levels of the monopole antenna drops dramatically, particularly at the room corners, while the dual-beam antenna can still maintain the RSSI levels above -58 dBm throughout the room for better communication service. The RSSI of the proposed dual-beam antenna exhibits slight asymmetry within Room 2 due to its non-static nature, which can be modeled as a Gaussian random variable [28], as well as the beam pointing errors caused by the possible non-ideal placement of the antenna.

The modulation and coding scheme index selected for throughput measurement is 11, which corresponds to 1024-

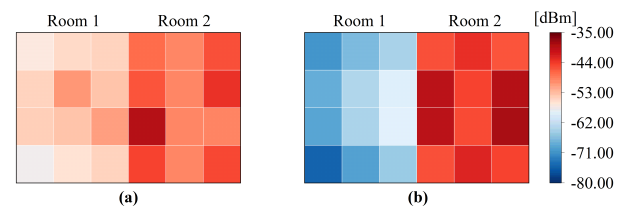


Fig. 11. RSSI distribution in Room 1 and Room 2 for (a) the proposed dual-beam antenna and (b) the monopole antenna.

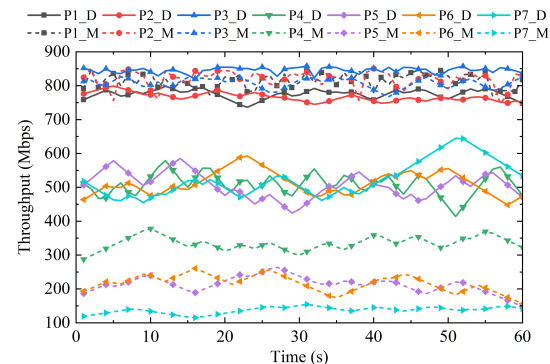


Fig. 12. Throughput results tested in one minute (D for the dual-beam antenna and M for the monopole antenna).

QAM modulation, as defined by the wireless network protocol IEEE 802.11ax. In this case, the maximum code rate is 5/6, the number of subcarriers is  $2 \times 980$ , and the maximum bandwidth is 160 MHz (one spatial stream), corresponding to a theoretical maximum throughput of 1201 Mbps. Usually, the actually measured throughput typically falls short of the theoretical limit, due to factors such as antenna performance, polarization mismatch, and ambient noise. The throughput measured at each sampling point is shown in Fig. 12. Although the throughput of the dual-beam antenna is slightly lower than that of the monopole at P1 and P2, it still exceeds 736 Mbps. In Room 1, the throughput of the dual-beam antenna are all greater than 414 Mbps, whereas the throughput of the monopole antenna gradually declines with distance and is less than 150 Mbps at P7. Overall, the proposed antenna demonstrates strong through-wall performance even under such high-attenuation conditions. For low attenuation environments such as plywood walls, using the proposed antenna would further enhance coverage, especially in multi-room or corner regions, due to the improved signal penetration capability.

## V. CONCLUSION

This letter proposes a high-gain dual-beam antenna with large beam tilt angle and broad bandwidth for through-wall FTTR applications. By generating two anti-phase electric currents within a single notch radiator, the dual-beam radiation is realized. Subsequently, two pairs of parasitic elements are introduced to achieve large beam tilt angle and broaden the bandwidth. The antenna performance is validated by impedance bandwidth and radiation pattern measurements. Furthermore, RSSI and throughput experiments are also conducted, demonstrating that the proposed antenna has excellent through-wall and multi-room coverage capabilities.

## REFERENCES

- [1] M. Wu, B. Zhang, Y. Zhou and K. Huang, "A Double-Fold  $7 \times 8$  Butler Matrix-Fed Multibeam Antenna With a Boresight Beam for 5G Applications," *IEEE Antennas Wireless Propag. Lett.*, vol. 21, no. 3, pp. 516-520, Mar. 2022.
- [2] K. Wu, Y. Yao, X. Cheng, J. Yu and X. Chen, "Design of Millimeter-Wave Circularly Polarized Endfire Antenna and Multibeam Antenna Array for Wireless Applications," *IEEE Trans. Antennas Propag.*, vol. 69, no. 12, pp. 8397-8406, Dec. 2021.
- [3] A. Dadgarpour, B. Zarghooni, B. S. Virdee and T. A. Denidni, "Single End-Fire Antenna for Dual-Beam and Broad Beamwidth Operation at 60 GHz by Artificially Modifying the Permittivity of the Antenna Substrate," *IEEE Trans. Antennas Propag.*, vol. 64, no. 9, pp. 4068-4073, Sep. 2016.
- [4] S. -Y. Yin and J. -L. Li, "Reconfigurable Antenna With Uni- and Bidirectional Radiation Patterns Based on Metasurface and Fresnel Zone Plate Lens," *IEEE Antennas Wireless Propag. Lett.*, vol. 23, no. 8, pp. 2291-2295, Aug. 2024.
- [5] T. Jia and X. Li, "A compact stacked bidirectional antenna for dual polarized WLAN applications," *Prog. Electromagn. Res. C*, vol. 44, pp. 95-108, 2013.
- [6] J. Hu, Z. -C. Hao, K. Fan and Z. Guo, "A Bidirectional Same Sense Circularly Polarized Endfire Antenna Array With Polarization Reconfigurability," *IEEE Trans. Antennas Propag.*, vol. 67, no. 11, pp. 7150-7155, Nov. 2019.
- [7] H. Guo and W. Geyi, "Design of Bidirectional Antenna Array With Adjustable Endfire Gains," *IEEE Antennas Wireless Propag. Lett.*, vol. 18, no. 8, pp. 1656-1660, Aug. 2019.
- [8] J. Hao, J. Ren, X. Du, J. H. Mikkelsen, M. Shen and Y. Z. Yin, "Pattern-Reconfigurable Yagi-Uda Antenna Based on Liquid Metal," *IEEE Antennas Wireless Propag. Lett.*, vol. 20, no. 4, pp. 587-591, Apr. 2021.
- [9] J. H. Kim and W. S. Park, "A Hadamard Matrix Feed Network for a Dual-Beam Forming Array Antenna," *IEEE Trans. Antennas Propag.*, vol. 57, no. 1, pp. 283-286, Jan. 2009.
- [10] X. G. Zhang, W. X. Jiang, H. W. Tian, Z. X. Wang, Q. Wang and T. J. Cui, "Pattern-Reconfigurable Planar Array Antenna Characterized by Digital Coding Method," *IEEE Trans. Antennas Propag.*, vol. 68, no. 2, pp. 1170-1175, Feb. 2020.
- [11] J. Hu, Z. -C. Hao and Y. Wang, "A Wideband Array Antenna With 1-Bit Digital-Controllable Radiation Beams," *IEEE Access*, vol. 6, pp. 10858-10866, 2018.
- [12] Y. Zhang, Z. Han, S. Tang, S. Shen, C. -Y. Chiu and R. Murch, "A Highly Pattern-Reconfigurable Planar Antenna With  $360^\circ$  Single- and Multi-Beam Steering," *IEEE Trans. Antennas Propag.*, vol. 70, no. 8, pp. 6490-6504, Aug. 2022.
- [13] Y. Fan et al., "Low-RCS Multi-Beam Metasurface-Inspired Antenna Based on Pancharatnam-Berry Phase," *IEEE Trans. Antennas Propag.*, vol. 68, no. 3, pp. 1899-1906, Mar. 2020.
- [14] Y. Hou, Y. Li, Z. Zhang and Z. Feng, "Dual-Beam Periodic Leaky-Wave Antenna With Reduced Beam Squinting," *IEEE Antennas Wireless Propag. Lett.*, vol. 18, no. 12, pp. 2533-2537, Dec. 2019.
- [15] C. Zhang, J. Ren, X. Du and Y. Yin, "Dual-Beam Leaky-Wave Antenna Based on Dual-Mode Spoof Surface Plasmon Polaritons," *IEEE Antennas Wireless Propag. Lett.*, vol. 20, no. 10, pp. 2008-2012, Oct. 2021.
- [16] Q. Zhang, Q. Zhang, H. Liu and C. H. Chan, "Dual-Band and Dual-Polarized Leaky-Wave Antenna Based on Slotted SIW," *IEEE Antennas Wireless Propag. Lett.*, vol. 18, no. 3, pp. 507-511, Mar. 2019.
- [17] F. Ge, H. Zhao, S. Li and X. Yin, "Bidirectional Scanning Antenna Based on Surface Wave Mode," *IEEE Antennas Wireless Propag. Lett.*, vol. 21, no. 8, pp. 1592-1596, Aug. 2022.
- [18] D. K. Karmokar, K. P. Esselle and T. S. Bird, "Wideband Microstrip Leaky-Wave Antennas With Two Symmetrical Side Beams for Simultaneous Dual-Beam Scanning," *IEEE Trans. Antennas Propag.*, vol. 64, no. 4, pp. 1262-1269, Apr. 2016.
- [19] A. Khidre, K. -F. Lee, A. Z. Elsherbeni and F. Yang, "Wide Band Dual-Beam U-Slot Microstrip Antenna," *IEEE Trans. Antennas Propag.*, vol. 61, no. 3, pp. 1415-1418, Mar. 2013.
- [20] C. Chen, Y. Guo and H. Wang, "Wideband Symmetrical Cross-Shaped Probe Dual-Beam Microstrip Patch Antenna," *IEEE Antennas Wireless Propag. Lett.*, vol. 14, pp. 622-625, 2015.
- [21] S. Liu, S. -S. Qi, W. Wu and D. -G. Fang, "Single-Feed Dual-Band Single/Dual-Beam U-Slot Antenna for Wireless Communication Application," *IEEE Trans. Antennas Propag.*, vol. 63, no. 8, pp. 3759-3764, Aug. 2015.
- [22] J. -F. Li, Z. N. Chen, D. -L. Wu, G. Zhang and Y. -J. Wu, "Dual-Beam Filtering Patch Antennas for Wireless Communication Application," *IEEE Trans. Antennas Propag.*, vol. 66, no. 7, pp. 3730-3734, Jul. 2018.
- [23] K. -D. Hong, X. Zhang, L. Zhu and T. Yuan, "A High-Gain and Pattern-Reconfigurable Patch Antenna Under Operation of  $TM_{20}$  and  $TM_{21}$  Modes," *IEEE Open J. Antennas Propag.*, vol. 2, pp. 646-653, 2021.
- [24] S. Cao, Z. Zhang, X. Fu and J. Wang, "Pattern-Reconfigurable Bidirectional Antenna Design Using the Characteristic Mode Analysis," *IEEE Antennas Wireless Propag. Lett.*, vol. 20, no. 1, pp. 53-57, Jan. 2021.
- [25] C. Chen, X. Xu, L. Zhang and F. Keshmiri, "Compact Horizontally Polarized Dual-Beam Antenna with Large Tilted Beam Angle for FTTR Applications," in *Proc. 19th Eur. Conf. Antennas Propag. (EuCAP)*, Mar. 2025, pp. 1-3.
- [26] C. A. Balanis, "Arrays: Linear, planar, and circular," in *Antenna Theory Analysis and Design*, 3rd ed. Hoboken, NJ, USA: Wiley, 2005, ch. 6, pp. 283-286.
- [27] B. Rohani, K. Takahashi, H. Arai, Y. Kimura and T. Ihara, "Improving Channel Capacity in Indoor  $4 \times 4$  MIMO Base Station Utilizing Small Bidirectional Antenna," *IEEE Trans. Antennas Propag.*, vol. 66, no. 1, pp. 393-400, Jan. 2018.
- [28] N. Patwari, A. O. Hero, M. Perkins, N. S. Correal, and R. J. O'Dea, "Relative location estimation in wireless sensor networks," *IEEE Trans. Signal Process.*, vol. 51, no. 8, pp. 2137-2148, Aug. 2003.